球铁光纤激光-MIG 复合焊接头的裂纹倾向与力学性能

郑世卿[1]， 温 鹏[1,2]， 单际国[1,2]
(1. 清华大学 机械工程系，北京 100084; 2. 清华大学 先进成形制造教育部重点实验室，北京 100084)

摘 要: 以 308L 不锈钢焊丝作为填充材料，采用光纤激光-MIG 电弧复合焊在 5 mm 厚的球墨铸铁上进行焊接，重点关注了工艺参数对裂纹倾向的影响，获得了成形良好且无裂纹的焊接接头. 结果表明，随着激光功率的减小和电弧电流的增加，接头熔合比减小，裂纹倾向降低. 接头显微硬度和组织的分析结果表明，由熔合比带来的碳含量变化是影响裂纹倾向的直接原因. 在厚度 10 mm 的球墨铸铁试件上开 X 形坡口进行多层多道焊，所得焊接接头的强度和断后伸长率分别为母材的 73% 和 20%，接头断裂机制为脆性断裂，半熔化区的莱氏体是造成断裂的原因.

关键词: 激光电弧复合焊; 球墨铸铁; 半熔化区组织; 裂纹; 力学性能
中图分类号: TG456.7 文献标识码: A 文章编号: 0253-360X(2012)08-0029-04

郑世卿

0 序 言

球墨铸铁具有良好的综合力学性能、优异的减震性能和低的成本，在风力发电、汽车制造等领域中有广泛应用[1]. 随着铸件结构的大型化和复杂化，一次铸造成形不仅成本高，而且极易产生缺陷，从而对球墨铸铁的焊接提出了要求. 然而球墨铸铁碳当量很高，在焊接过程中大量碳溶解进入熔池中，在焊后的快速冷却过程中以莱氏体的形式析出，引起冷裂纹和力学性能恶化等问题[2-4].

激光热源具有能量密度集中、热输入小等优势，可以减少母材的熔化，降低熔池碳含量，作为球墨铸铁焊接的热源具有较大优势，但是目前关于球墨铸铁激光焊的研究很少. 德国亚琛大学 Dilthey 等人[5,6]研究了球墨铸铁与钢异种接头的激光焊接，认为添加含镍的填充材料有利于提高接头的性能，但未就工艺参数对焊接接头的裂纹倾向的影响规律和机理进行深入分析.

文中采用光纤激光-MIG 电弧复合焊在球墨铸铁上进行焊接，重点关注了复合焊工艺参数对裂纹倾向的影响及其作用机理，并对接头的力学性能进行了测试，旨在发展一种优质高效的球墨铸铁连接方法.

收稿日期: 2011-06-07
基金项目: 国家自然科学基金资助项目(51005125)

1 试验方法

母材为 400 MPa 级的球墨铸铁，化学成分(质量分数)为 3.71% C，2.08% Si，0.163% Mn，0.039% Mg，Fe 为余量，抗拉强度为 379 MPa，断后伸长率为 12.7%. 308L 奥氏体不锈钢焊丝作为填充材料.

图 1 为使用的激光-MIG 电弧复合焊焊矩. 采用 IPG YLS-2000 光纤激光器作为光源，波长为 1.07 μm，聚焦光斑直径约为 0.13 mm. 移动轨迹通过四轴三联动的机床实现. 采用激光-MIG 复合焊在尺寸为 110 mm × 40 mm × 5 mm 的母材上进行平板堆焊试验，焊接工艺参数如表 1 所示. 焊后对接头的表面裂纹、熔合比、显微硬度和组织进行分析. 根据平板堆焊获得的优化参数，在尺寸为200 mm ×

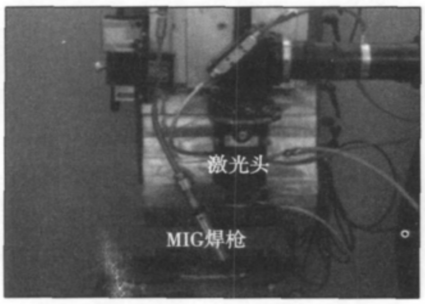

图 1 激光-MIG 电弧复合焊接系统
Fig. 1 Laser-MIG hybrid welding system

110 mm × 10 mm 的母材上开 X 形坡口进行多层多道焊，焊后根据国家标准 GB/T 2651—2008 制作接头的拉伸试样，并进行拉伸试验.

表 1 激光-MIG 复合焊工艺参数

Table 1 Parameters of laser-MIG hybrid welding

试样编号	激光功率 P/W	焊接电流 I/A	电弧电压 U/V	焊接速度 v/(mm·s^{-1})
J1	2 000	32	13	8.3
J2	1 600	32	13	8.3
J3	1 600	60	16	8.3
J4	800	60	16	8.3
J5	1 600	90	18	8.3
J6	800	90	18	8.3

2 试验结果与分析

2.1 工艺参数对裂纹倾向的影响

平板堆焊接头着色渗透探伤结果如图 2 所示. J1 表面存在大量裂纹，J2 表面有少量裂纹，J3-J6 表面未发现裂纹. 说明接头裂纹倾向随着激光功率的降低和焊接电流的增加而降低，当焊接电流不小于 60 A 时，接头不产生裂纹.

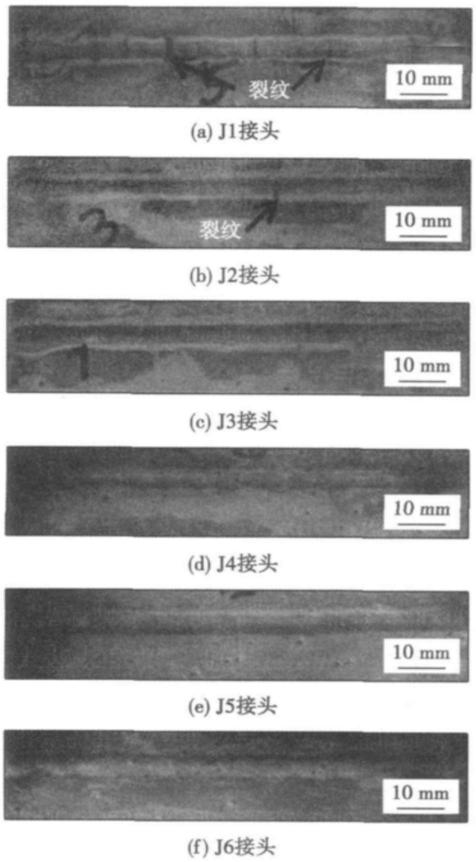

图 2 平板堆焊接头的着色探伤结果

Fig. 2 Dye penetration of joints on plate

2.2 焊缝横截面宏观形貌与显微硬度分布

高功率和低功率接头(分别以 J1 和 J4 为代表)的横截面形状如图 3 所示. 测试了各个接头的熔合比，如表 2 所示. J1 的激光功率较高、电流较小、接头熔深大、堆高小、熔合比大. J2，J3，J5 的横截面形貌与 J1 相似. J4 的激光功率较小、电流较大、接头熔深小、堆高大、熔合比小. J6 的横截面形貌与 J4 相似. 由以上结果可知，激光功率减小，母材熔化量减小，熔合比减小; 焊接电流增加，焊丝填充量增加，熔合比减小. 结合图 2 可知，熔合比减小导致接头裂纹倾向随之降低，当熔合比不超过 58% 时，接头没有裂纹产生.

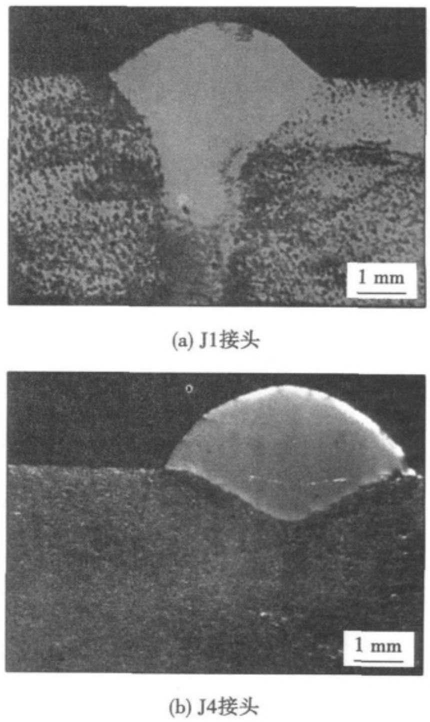

图 3 平板堆焊接头的横截面形貌

Fig. 3 Cross section of joints on plate

表 2 焊缝熔合比

Table 2 Penetration ratio

试样编号	熔合比 D(%)	试样编号	熔合比 D(%)
J1	75	J2	69
J3	58	J4	32
J5	40	J6	25

对不同参数下获得的平板堆焊接头的横截面进行了熔宽和熔深方向的显微硬度分布测试，其硬度分布如图 4 所示. 从图 4a，b 可以看出 J1，J3 和 J4

的熔合线附近都存在 800 HV 左右的硬度峰值；J4 焊缝熔深方向硬度分布均匀，约为 350 HV．从图 4c 可以看出，J1 和 J3 自焊缝顶部至底部硬度逐渐升高，顶部硬度约为 450 HV，底部硬度可达 800 HV 左右，J1 焊缝的硬度大于 J3．

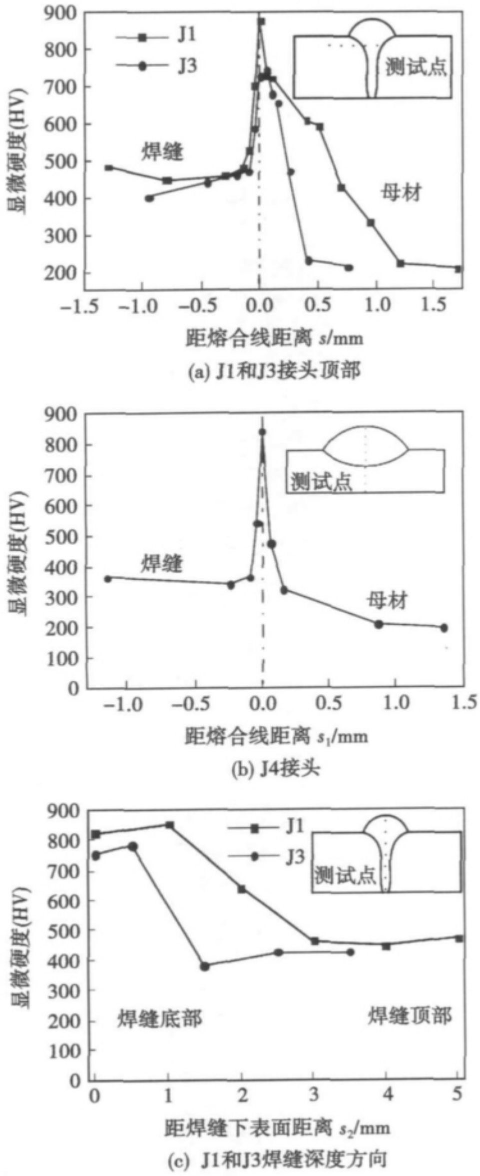

图 4　平板堆焊接头的硬度分布
Fig. 4　Hardness distribution in joints on plate

2.3　焊接接头的微观组织

典型焊接接头的微观组织形貌如图 5 所示，结合显微硬度的分布，对接头中的组织进行了分析．J4 整个焊缝为均一的奥氏体组织（图 5a）．J1 焊缝上部为奥氏体组织（图 5b）；J1 下部焊缝为奥氏体和莱氏体的混合组织（图 5c）；J2，J3，J5 的焊缝组织与 J1 相似，J6 的焊缝组织与 J4 相似．所有接头中半熔化区（PMZ）的组织均为莱氏体组织和残余石墨，图 5d 所示为 J1 接头 PMZ 的组织．

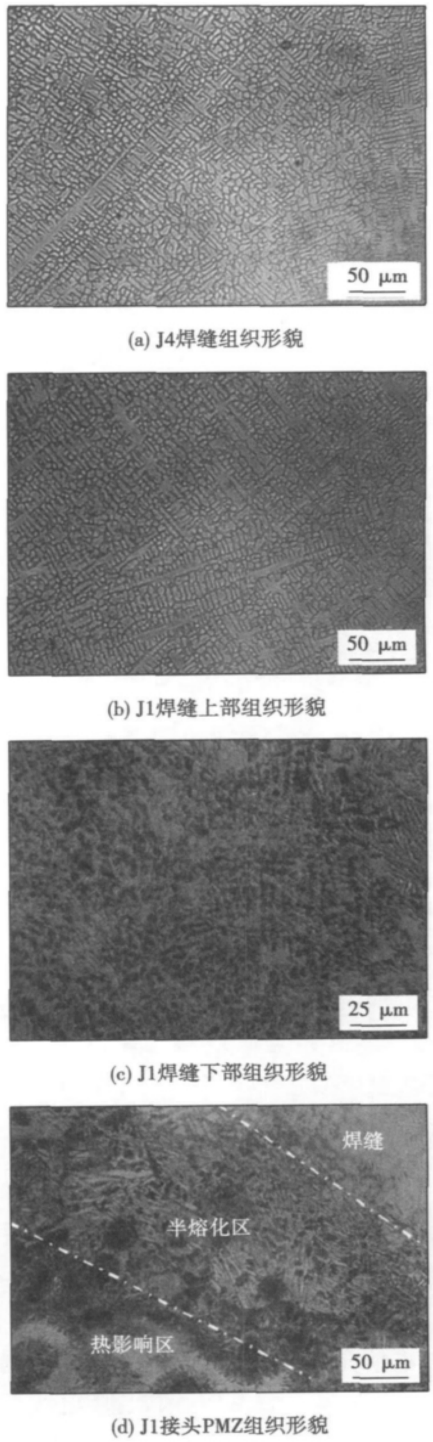

图 5　平板堆焊接头的显微组织形貌
Fig. 5　Microstructure of joints on plate

结合接头裂纹倾向、熔合比和显微硬度可知，熔合比减小引起焊缝碳含量减少，焊缝中的莱氏体含量减小，显微硬度下降，接头裂纹倾向也随之降低．即由熔合比带来的碳含量变化是影响裂纹倾向的直

接原因.

2.4 拉伸性能

利用平板堆焊接头J4的工艺参数进行10 mm厚板的多层多道焊,焊后对所得接头的拉伸性能进行测试,平均抗拉强度为271.6 MPa,平均断后伸长率为2.2%,分别为母材强度和断后伸长率的73%和20%. 断裂主要是沿熔合线发生的,如图6a所示. 断口呈亮色,为解理状断裂,断口表面分布有少量的韧窝,如图6b所示. 结合平板堆焊的组织分析,解理型断口主要由莱氏体引起的;少量韧窝可能由残余石墨导致. 焊接接头的莱氏体组织在拉伸过程中成为断裂源,导致脆性断裂的发生,是力学拉伸性能下降的主要原因,因此抑制莱氏体的形成是进一步提高接头力学性能的关键.

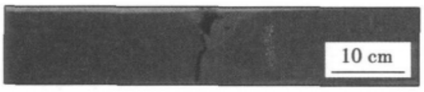

(a) 断裂位置

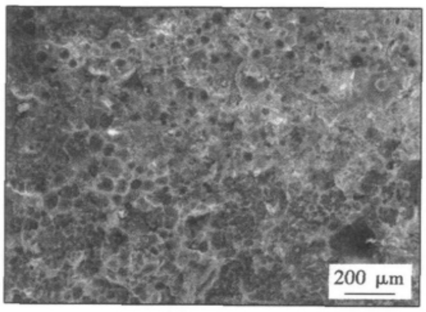

(b) 断口形貌

图6 拉伸试样断裂分析

Fig. 6 Fracture analysis of tensile test piece

3 结 论

(1) 随着激光功率的减小和焊接电流的增加,接头熔合比减小,裂纹倾向降低. 当电流不小于60 A时,熔合比不大于58%,接头不产生裂纹.

(2) 由熔合比带来的碳含量变化是影响裂纹倾向的直接原因. 减小激光功率和增加电流都会降低焊接熔池的碳含量,减少莱氏体的生成,从而降低接头裂纹倾向.

(3) 在10 mm板上开X形坡口进行双面激光–MIG复合焊接,获得了成形良好无裂纹的焊接接头,接头强度和断后伸长率分别为母材的73 %和20 %,进一步抑制莱氏体的形成是提高接头力学性能的关键.

参考文献:

[1] Roedter H, Gagne M. Ductile iron for heavy section wind mill castings: a European experience [C] // The Ductile Iron Society. Keith Millis Symposium on Ductile Cast Iron. Hilton Head Island: American Foundrymen's Society, 2003: 22–28.

[2] Klimpel A. The problem of welding cast irons is examined taking the example of a spheroidal cast iron [J]. Welding International, 1998, 12(1): 20–24.

[3] 彭高娥. 球墨铸铁焊接和焊接材料的国内外现状 [J]. 焊接, 1987(1): 10–12.
Peng Gaoe. Researchsituation of home and abroad of ductile cast iron welding and welding material [J]. Welding & Joining, 1987(1): 10–12.

[4] 周振丰. 国内外铸铁焊接研究及应用现状 [J]. 焊接, 1982(2): 1–4.
Zhou Zhenfeng. Research andapplication situation of home and abroad of cast iron welding [J]. Welding & Joining, 1982(2): 1–4.

[5] Dilthey U, Bohm S, Trager G, *et al*. Laser-beam and electron-beam welding of material combinations consisting of cast iron and case-hardening or heat-treatable steels [J]. Welding and Cutting, 1998, 50(7): 214–216.

[6] Dilthey U, Risch A, Shu X. Laser welding of the material combinations cast iron alloys (spheroidal graphite cast iron GGG and malleable cast iron GTS) and steels [C] // PRC. Proceedings of the 27th International Symposium on Automotive Technology and Automation. Aachen: Pergamon Press Ltd, 1994: 383–385.

作者简介: 郑世卿,男,1985年出生,博士研究生. 主要从事激光焊接方面的研究. 发表论文5篇. Email: zsq03@mails.tsinghua.edu.cn

通讯作者: 单际国,男,教授,博士研究生导师. Email: shanjg@mail.tsinghua.edu.cn

maximum value of the first main stress in the copper columns and joints appeared in the edge corner of the lowest layer, and the maximum stress in the chips appeared in the inner surface of the TSV. In order to simulate the influence of structure parameters on the residual stress, the orthogonal test with three factors and three levels was designed using the maximum stress of the joints as the response. The three main factors influencing the residual stress in the package, the resin thickness, the chip thickness and the resin hardness, were chosen to be the parameters of the package structure. The results showed that the resin thickness played the most important role but the resin hardness played the least important role in affecting the stress in the joint.

Key words: 3D package; intermetallic compound joint; finite element simulation; parameter optimization

On-site turbine blade repairing robot with self-positioning function MA Xiande, CHEN Qiang, SUN Zhenguo, ZHANG Wenzeng (Key Laboratory for Advanced Materials Processing Technology, Ministry of Education, Tsinghua University, Beijing 100084, China). pp 21 – 24

Abstract: A type of mobile robot with self-positioning function was developed to accomplish the task of repairing large turbine blades with complex curved surface in closed on-site environment. The robot system consisted of a gapped-adhesive mobile platform, a multi-degree-of-freedom manipulator and a multi-functional operation unit. It can reliably adhere to the blade while flexibly moving on the blade surface, and complete all-position welding, air gouging and grinding tasks. The hardware platform of the self-positioning system was built using the inclinometer to adjust the pose information acquired by the inertial navigating method, and using the geometric feature of the blade surface to adjust the position information acquired by the odometry method. The experiments on the simulating blade showed that the pose error was less than 0.5° and the position error was around 35 mm, which can satisfy the self-positioning precision requirement of the blade-repairing tasks.

Key words: turbine blade; welding; mobile robot; self-positioning; geometric adjustment

Laser cladding of in-situ TiB_2-TiC particles reinforced Fe-based coatings WANG Xinhong, ZOU Zengda, QU Shiyao (Key Laboratory for Liquid-Solid Structural Evolution and Processing of Materials, Ministry of Education, Shandong University, Jinan 250061, China). pp 25 – 28

Abstract: In-situ TiB_2-TiC particles reinforced Fe-based coatings were produced on carbon steel substrate by laser melting of mixture of B_4C, TiO_2, graphite and Fe-based self-melting alloy powders. The phase structure and microstructure was investigated with XRD and SEM. Meanwhile, the microhardness and wear properties of the coatings were tested with the micro-vickers and block-on-ring wear testing machine. The results showed that TiB_2 and TiC ceramic particles were synthesized from the reaction of $B_4C + TiO_2 + C$ during laser cladding process, and the TiB_2 and TiC particles were uniformly distributed in the coating. The amount of TiC decreased with the increase of laser power density. The microhardness and wear resistance of coatings were higher than those of 45 steel substrate.

Key words: TiB_2-TiC particles; laser cladding; microstructure; wear property

Crack tendency and mechanical properties of ductile cast iron joint by fiber laser-MIG hybrid welding ZHENG Shiqing[1], WEN Peng[1,2], SHAN Jiguo[1,2] (1. Department of Mechanical Engineering, Tsinghua University, Beijing 100084, China; 2. Key Laboratory for Advanced Materials Processing Technology, Ministry of Education, Tsinghua University, Beijing 100084, China). pp 29 – 32

Abstract: Fiber laser-pulsed MIG hybrid welding of 5 mm-thick ductile cast iron sheet was conducted with 308L stainless steel wire as the filler metal. The effect of welding parameters on cracking tendency was discussed, and joints with good formation and no cracks were obtained. The results showed that penetration ratio decreased with increasing welding current and decreasing laser power, which subsequently decreased the crack tendency. Based on hardness and microstructure analysis, the change of carbon content induced by penetration ratio was the direct reason for crack tendency. Multi-layer and multi-pass welding was carried out on 10 mm-thick ductile cast iron plate using the optimized parameters, and the tensile strength and elongation of the resultant joints reached 73% and 20% of those of the base metal, respectively. The existence of ledeburite in partially melting zone resulted in the brittle fracture of the joints.

Key words: laser-arc hybrid welding; ductile cast iron; partially melting zone; crack; mechanical properties

Effect of thermal exposure on microhardness and element distribution in welding interface of Ti-24Al-15Nb-1.5Mo/TC11 dual alloys QIN Chun[1], YAO Zekun[1], ZHOU Wei[1], GUO Hongzhen[1], CAO Jingxia[2] (1. School of Materials Science and Engneering, Northwestern Polytechnical University, Xi'an 710072, China; 2. Titanium Alloys Laboratory, Beijing Institute of Aeronautical Materials, Beijing 100095, China). pp 33 – 36

Abstract: Microhardness and element distribution in the welding interface of Ti-24Al-15Nb-1.5Mo/TC11 dissimilar alloys was investigated through thermal exposure experiment at 550 ℃ for 50 h. The results showed that the microhardness of Ti-24Al-15Nb-1.5Mo alloy after gradient heat treatment was higher than that after double heat treatment. Under gradient heat treatment, the decrease of acicular α phases in weld seam with 30% deformation resulted in increase of the microhardness, while the microhardness in Ti-24Al-15Nb-1.5Mo alloy decreased due to the release of lattice distortion energy. However, the microhardess in the welded joints under 40%, 50% deformation and gradient heat treatment decreased after thermal exposure because of the decomposing and growing of phases in the seam. Elements in the welding interface continued diffusing during thermal exposure experiment. The lattice distortion increased as Nb content increased significantly in the weld seam after thermal exposure, which also resulted in the increase of the microhardness.

Key words: dual alloys; microhardness; elemental diffusion

Shape design of reinforcement for under-matched butt joints under three-point bending load in elastic stage WANG Jiajie[1,2], DONG Zhibo[1], LIU Xuesong[1], FANG Hong yuan[1], GANG Tie[1] (1. State Key Laboratory of Advanced Welding and Joining, Harbin Institute of Technology, Harbin 150001, China; 2. School of Materials and Chemical Engineering, Heilongjiang Institute of Technology, Harbin 150050, China). pp 37 – 40